The International Journal of Advanced Manufacturing Technology (2024) 131:1989–2000
https://doi.org/10.1007/s00170-022-10524-5

ORIGINAL ARTICLE

Study on the influence of ultrasonic-assisted cutting on the surface quality of CFRP

Xiaobo Wang[1] · Chaosheng Song[1] · Jinglin Tong[1] · Lulu Li[1] · Mingqiang Wu[1] · Bo Zhao[1]

Received: 26 October 2022 / Accepted: 10 November 2022 / Published online: 25 November 2022

Abstract
In order to study the influence of machining methods and parameters on the surface quality of carbon fiber reinforced composites (CFRP) in the cutting process, the finite element simulation model of ultrasonic-assisted cutting CFRP was established, the simulation results show that the introduction of ultrasonic reduces the damage degree of CFRP in the cutting process, and the tool attached torsional ultrasonic vibration effect is the most significant. The ultrasonic-assisted torsion and longitudinal cutting tests of CFRP disc were carried out respectively, and compared with the ordinary cutting process, the experimental results show that the introduction of ultrasonic changes the fracture mode of fiber and effectively reduces the surface roughness. The fiber cutting angle (the angle between the cutting speed direction and the fiber direction) is the main factor affecting the surface roughness of CFRP, the effect of ultrasonic is better in the low-speed area, and the direction of fiber can be weakened by high-speed processing. When the amplitude is in the range of 0 ~ 6 μm, with the increase of amplitude, the advantage of ultrasonic is more obvious, and the inhibition of the influence of fiber directivity is more obvious. The results show that large amplitude and small cutting speed can achieve better ultrasonic machining effect; large vibration amplitude and high cutting speed can effectively suppress the influence of fiber directivity. The results are helpful for the high-quality processing of CFRP and other composite materials.

Keywords Carbon fiber–reinforced composites · Ultrasonic-assisted cutting · Finite element simulation · Surface quality

1 Introduction

Composite material is a new type of high performance material obtained by a series of processing processes of some reinforcing phase materials and matrix materials, which is a new type of low density thermal structure material rapidly developed in recent years [1]. Compared with ordinary metal materials, composite materials have the advantages of low density, high strength, and low coefficient of thermal expansion and have been widely used in the aerospace field [2]. The consumption of composite materials for the body of the new generation of large civil aircraft has increased from 2% of the whole machine quality in 1950 to about 50% at present and is mainly used in the manufacture of core parts of key parts of aircraft [3]. CFRP has gradually become the leading material in key parts of the aviation field [4]. Usually, CFRP is made by "near net forming" process; the structure and materials of complex components are designed and manufactured in an integrated way, so as to improve processing efficiency and reduce assembly steps; however, in order to make the components meet the geometric dimension and shape accuracy required by the parts, the secondary processing after material forming is inevitable [5]. The defects such as delamination, burr, and edge collapse are easily produced by the traditional secondary processing, which seriously affect the quality and performance of processed CFRP [6]. Therefore, the study on how to improve the processing quality and comprehensive performance of CFRP has certain guiding significance for the application of CFRP in the industrial field.

In recent years, many experts have conducted many corresponding studies on ultrasonic-assisted machining; the main components of ultrasonic system include ultrasonic power supply, transducer, and horn [7, 8]. Ultrasonic-assisted cutting is a combination of ultrasonic vibration machining technology and traditional cutting, in order to achieve better machining results [9]. Ultrasonic-assisted cutting changes the material removal mechanism, effectively increasing the material removal rate, reducing cutting force, cutting heat, reducing tool wear, and improving machining accuracy and quality [10, 11]. Wang et al. [12] established the grinding force model of horizontal ultrasonic vibration grinding CFRP

✉ Xiaobo Wang
wangxb@hpu.edu.cn

1 School of Mechanical and Power Engineering, Henan Polytechnic University, Jiaozuo 454000, People's Republic of China

and found that the grinding force decreased with the increase of ultrasonic amplitude. Patil et al. [13] conducted finite element simulation and experimental research on ultrasonic-assisted cutting of Ti6Al4V and found that the introduction of ultrasonic can significantly reduce the cutting force and reduce the cutting temperature. Muhammad et al. [14] conducted ultrasonic-assisted grinding experiments on SiCp/Al, and the results showed that compared with traditional grinding, ultrasonic-assisted grinding can improve the surface quality of materials. Liu et al. [15] found that the introduction of ultrasonic can significantly improve the quality of machined edges through ultrasonic-assisted milling of carbon fiber–reinforced silicon carbide matrix composites. Through the research of the above scholars, it is found that ultrasonic-assisted processing has better processing effect than traditional processing. In this paper, ultrasonic-assisted cutting is introduced to improve the surface quality of CFRP.

Compared with isotropic traditional metal materials, the structural heterogeneity and mechanical anisotropy of CFRP materials lead to more complex removal process, worse machinability, and more serious damage on the machined surface [16]. The influence of the non-uniformity of CFRP structure in the cutting process is mainly manifested in the interaction between the reinforced base fiber and the matrix resin alternately and the cutting edge of the tool; however, the removal mechanism of fiber and resin is completely different, so under the action of the same cutting edge, the fiber is easy to pull out, the resin is easy to fall off, and the laminates between layers are easy to produce delamination, tearing and other damage, which will directly affect the quality of the processed surface [17]. Lou et al. [18] found through grinding tests on carbon fiber composites that fiber angle has a great impact on roughness, and the damage form also changes with the change of fiber angle. Chen et al. [19] conducted experiments on ultrasonic-assisted milling of 2D C_f/SiC composites and found that appropriate amplitudes promoted material removal and reduced the roughness of the machined surface. IK [20] conducted orthogonal cutting experiments with unidirectional glass fiber–reinforced composites and studied the correlation between the machined surface roughness and the geometric parameters of the tool, cutting speed, cutting depth, and other parameters. After that, IK et al. [21] proposed a new method to optimize cutting parameters and verified the correctness of the optimization method by drilling braided composites. It can be seen from the above that the machining parameters have a close influence on the surface quality.

To sum up, ultrasonic vibration is a very effective technology for machining composite materials. At present, the research on ultrasonic vibration turning CFRP mostly focuses on the optimization of parameters and the improvement of processing technology, while the research on the material removal mechanism of ultrasonic vibration cutting CFRP is very small. In the process of ultrasonic-assisted cutting of CFRP, the introduction of ultrasonic vibration changes the force, energy, motion track, etc. between the tool and the workpiece, which is bound to affect the removal mechanism of CFRP in the cutting process and then affect the surface quality of CFRP; attention should be paid to this research direction. This paper intends to reveal the influence mechanism of processing methods and processing parameters on surface quality through the combination of experiment and simulation.

2 Establishment of finite element simulation model

2.1 Establishment of constitutive model

CFRP is composed of reinforcing fiber and matrix resin, and its mechanical properties are much more complex than metal materials due to anisotropy. From the microscopic scale, the resin matrix of CFRP is elastoplastic, while the reinforced fiber is brittle. From the macroscopic scale, CFRP is composed of several layers of unidirectional laminates bonded through the matrix at different angles. Therefore, CFRP is a typical anisotropic material, and its material should meet the constitutive relation of Eq. (1) [22].

$$\begin{bmatrix} \sigma_x \\ \sigma_y \\ \sigma_z \\ \sigma_{yz} \\ \sigma_{zx} \\ \sigma_{xy} \end{bmatrix} = \begin{bmatrix} \sigma_1 \\ \sigma_2 \\ \sigma_3 \\ \sigma_4 \\ \sigma_5 \\ \sigma_6 \end{bmatrix} = \begin{bmatrix} C_{11} & C_{12} & C_{13} & 0 & 0 & 0 \\ C_{21} & C_{22} & C_{23} & 0 & 0 & 0 \\ C_{31} & C_{32} & C_{33} & 0 & 0 & 0 \\ 0 & 0 & 0 & C_{44} & 0 & 0 \\ 0 & 0 & 0 & 0 & C_{55} & 0 \\ 0 & 0 & 0 & 0 & 0 & C_{66} \end{bmatrix} \cdot \begin{bmatrix} \varepsilon_1 \\ \varepsilon_2 \\ \varepsilon_3 \\ \varepsilon_4 \\ \varepsilon_5 \\ \varepsilon_6 \end{bmatrix} \quad (1)$$

where 1, 2, and 3 respectively represent the three directions of x, y, and z axis; C_{ij} represents the stiffness matrix component, and $i, j = 1 \sim 6$; σ_i is the stress component; ε_i is the strain component. The stiffness matrix is expressed as Eq. (2).

$$\begin{cases} C_{11} = \frac{1-\nu_{23}\nu_{32}}{E_2E_3\Delta} \\ C_{12} = \frac{\nu_{12}+\nu_{13}\nu_{32}}{E_2E_3\Delta} = \frac{\nu_{21}+\nu_{31}\nu_{23}}{E_1E_3\Delta} \\ C_{13} = \frac{\nu_{13}+\nu_{12}\nu_{23}}{E_2E_3\Delta} = \frac{\nu_{31}+\nu_{21}\nu_{32}}{E_1E_2\Delta} \\ C_{22} = \frac{1-\nu_{13}\nu_{31}}{E_1E_3\Delta} \\ C_{23} = \frac{\nu_{23}+\nu_{21}\nu_{13}}{E_2E_3\Delta} = \frac{\nu_{32}+\nu_{12}\nu_{31}}{E_1E_2\Delta} \\ C_{33} = \frac{1-\nu_{12}\nu_{21}}{E_1E_2\Delta} \\ C_{44} = G_{23}, C_{55} = G_{13}, C_{66} = G_{12} \\ \Delta = \frac{1-\nu_{12}\nu_{21}-\nu_{23}\nu_{32}-\nu_{13}\nu_{31}-2\nu_{12}\nu_{23}\nu_{31}}{E_1E_2E_3} \end{cases} \quad (2)$$

E_1, E_2, and E_3 are tensile-compressive modulus in the x, y, and z axes respectively; G_{12}, G_{13}, and G_{23} are the shear modulus in xy, xz, and yz directions respectively; v_{12}, v_{13}, v_{23} are Poisson's ratios in xy, xz, and yz directions respectively.

The failure modes of carbon fiber–reinforced composites, such as fiber fracture, interlayer delamination, and fiber-matrix debonding, have the same characteristics under dynamic and static loads. The failure criterion under quasi-static analysis can be used for reference in the analysis considering the strain rate effect of composite materials [23, 24]. The damage and failure of CFRP are generally divided into two forms: interlaminar damage and interlaminar damage; the interlaminar damage includes fiber fracture and matrix cracking. In this section, the Hashin failure criterion [25] provided by the ABAQUS finite element software is used to establish the simulation model of CFRP. Four failure modes mainly include the following: tensile damage and compression damage of fibers, cracking and crushing of matrix [26, 27].

The tensile damage and compressive damage of fibers are dominated by axial stress, where the fiber stretch $\left(\sigma_{11} < 0\right)$ and the fiber compression $\left(\sigma_{11} < 0\right)$ The initial damage to the fiber usually occurs in the tangential section of the fiber and then rapidly spreads throughout the fiber cross section, eventually causing tensile or fracture failure of the fiber material. The expression of failure factor criterion is:

$$F_f^t = \left(\frac{\sigma_{11}}{X_T}\right)^2 + \left(\frac{{\sigma_{12}}^2 + {\sigma_{13}}^2}{{S_C}^2}\right)^2 = 1 \tag{3}$$

$$F_f^c = \left(\frac{\sigma_{11}}{X_C}\right)^2 = 1 \tag{4}$$

The tensile cracking and crushing damage of matrix are mainly caused by the coupling effect of transverse stress σ_{22} and plane shear stress σ_{12}, in which the matrix tensile damage $(\sigma_{22} + \sigma_{33} \geq 0)$, compression damage of the matrix $(\sigma_{22} + \sigma_{33} \geq 0)$. The expression of failure factor criterion is:

$$F_m^T = \left(\frac{\sigma_{22} + \sigma_{33}}{Y_T}\right)^2 + \frac{{\sigma^2}_{23} + \sigma_{22} \cdot \sigma_{33}}{{S_T}^2} + \frac{\sigma_{12}^2 + \sigma_{13}^2}{{S_C}^2} = 1 \tag{5}$$

$$F_m^C = \left(\frac{\sigma_{22}+\sigma_{33}}{2 \cdot S_T}\right)^2 + \left[\left(\frac{Y_C}{2 \cdot S_C}\right)^2 - 1\right] \cdot \frac{\sigma_{22}+\sigma_{33}}{Y_C} + \frac{{\sigma_{23}}^2 - \sigma_{22} \cdot \sigma_{33}}{{S_T}^2} + \frac{\sigma_{12}^2+\sigma_{13}^2}{{S_C}^2} = 1 \tag{6}$$

σ_{11} is the stress in the fiber direction, σ_{22} is the stress in the shear direction, σ_{12} is the in-plane shear stress, X_C is the compressive strength in the fiber direction, X_T is the tensile strength in the fiber direction, Y_T is the transverse tensile strength perpendicular to the fiber direction, Y_C is the transverse compressive strength perpendicular to the fiber direction, S_T is the in-plane fiber direction shear strength, S_C is the transverse shear strength perpendicular to the fiber, F_f^t is the fiber compression fracture energy, F_f^c is the tensile breaking energy of the fiber, F_m^T is the tensile fracture energy of the matrix, and F_m^c is the compressive fracture energy of the matrix.

The process from damage to complete failure of CFRP is a gradual accumulation; therefore, after the failure is judged by Hashin criterion, the damage factor of CFRP is introduced according to Matzenmiller's research results [28]. The corresponding damage stiffness matrix can be expressed by Eq. (8).

$$C(d) = \frac{1}{\Delta} \tag{7}$$

$$\begin{bmatrix} d_f C_{11} & d_f d_m C_{12} & d_f d_m C_{13} & 0 & 0 & 0 \\ & d_m C_{22} & d_m C_{23} & 0 & 0 & 0 \\ & & C_{33} & 0 & 0 & 0 \\ & & & d_m C_{44} & 0 & 0 \\ & & & & d_f C_{55} & 0 \\ & & & & & d_f d_m C_{66} \end{bmatrix} \tag{8}$$

The global damage variable of fiber failure is $d_f = \left(1 - d_{ft}\right)\left(1 - d_{fc}\right)$; the damage factors corresponding to fiber tension and fiber compression are d_{ft}, d_{fc}. The global damage variable of matrix failure is $d_m = \left(1 - d_{mt}\right)\left(1 - d_{mc}\right)$; the damage factors corresponding to matrix tension and matrix compression are d_{mt}, d_{mc}. Table 1 shows the performance parameters used in the simulation.

The explicit module of ABAQUS/CAE finite element analysis software is used to simulate the cutting process. Through programming language, uniformly distributed reinforced carbon fibers are generated in the resin matrix, the volume of reinforcing phase accounts for 60% of the total composite, and the average fiber diameter is 7 µm. To simulate the real material cutting process, a cohesive element is added between the matrix and the reinforcement phase to simulate the interfacial phase. The tool is constrained into a rigid body with a front angle of 5° and a back angle of 7°, set the tangential friction coefficient to 0.2 in the contact setting, add the speed V_t=40 m/min in the load setting, and the ultrasonic vibration is characterized by the periodic amplitude function. In order to balance the relationship between the simulation time and the accuracy of the simulation results, the meshes near the machining tool and the workpiece interface layer are refined.

2.2 Micro simulation of ultrasonic-assisted cutting CFRP

The anisotropic mechanical properties of CFRP lead to the significant influence of machining mode on the surface

Table 1 Mechanical properties of CFRP (T300) [29, 30]

Material property parameters	Numerical value	Material property parameters	Numerical value
Tension compression modulus E_1/MPa	135,000	Shear modulus G_{12}/MPa	4590
Tension compression modulus E_2/MPa	8500	Shear modulus G_{13}/MPa	4590
Tension compression modulus E_3/MPa	8500	Shear modulus G_{23}/MPa	2900
Poisson's ratio ν_{12}	0.3	Longitudinal tensile strength X_T/MPa	1298
Poisson's ratio ν_{13}	0.3	Longitudinal compressive strength X_C/MPa	1068
Poisson's ratio ν_{23}	0.45	Transverse tensile strength Y_T/MPa	64
Shear strength S_{12}/MPa	96	Transverse compressive strength Y_C/MPa	185
Shear strength S_{13}/MPa	96	Interlaminar tensile strength Z_T/MPa	64
Shear strength S_{23}/MPa	84	Layer compressive strength Z_C/MPa	185

morphology. The cutting force clouds and damage levels for 90° orthogonal cutting of 0° layered CFRP with different machining methods and the same cutting parameters (V_t = 40 m/min, f = 35 kHz, A = 4 μm) are given in Fig. 1. Where V_t is the cutting speed of the tool, f is the frequency of ultrasonic vibration, and A is the amplitude of ultrasonic vibration. In Fig. 1b, the additional torsional vibration of the tool reduces the average normal force, which shows that the color of stress distribution in the whole cutting force cloud is the lightest, and only a small area of dark color appears in the most front of the cutting edge; due to the effect of ultrasonic impact force, the instantaneous energy of cutting edge is higher, which leads to the fracture of the cut fiber in the form of broken before bending, and even the hole appears in the front of the tool tip, indicating that the torsional vibration of the tool changes the fracture mode of the fiber. In Fig. 1c, the additional longitudinal vibration of the tool makes periodic contact and separation between the tool and the workpiece, which reduces the cutting force and cutting heat and increases the impact of the tool on the

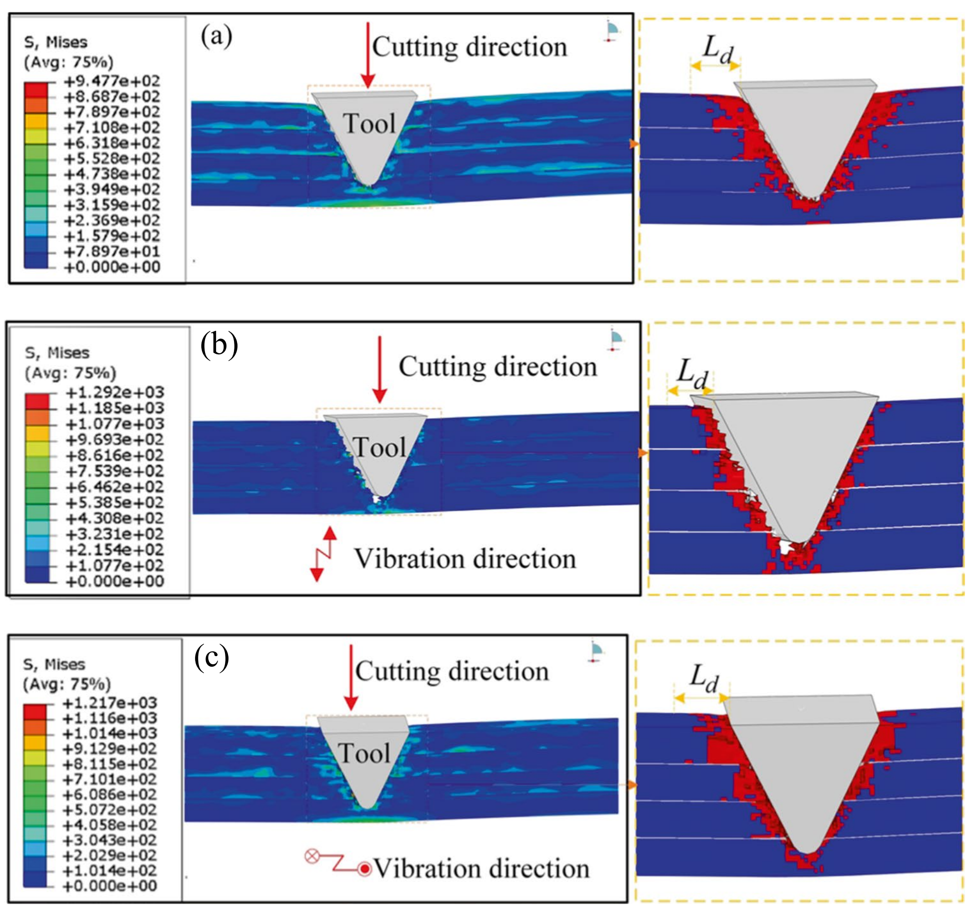

Fig. 1 CFRP cutting force nephogram and damage (θ = 90°). **a** Ordinary cutting. **b** Torsional ultrasonic-assisted cutting. **c** Longitudinal ultrasonic-assisted cutting

workpiece, which is helpful for the removal of materials and the discharge of chips, while the cloud (Fig. 1a) of the cutting force cloud for conventional machining has a relatively dark color of stress distribution and a wide range of stress diffusion. The reason for this is that the cutting forces on both sides of the tool exceed the critical limit of delamination during conventional machining, which in turn leads to serious delamination.

In order to quantitatively study the influence of cutting mode and fiber cutting angle on the damage degree of CFRP, finite element cutting simulations were performed for CFRP with four different fiber cutting angles ($\theta = 0°$, $\theta = 45°$, $\theta = 90°$, $\theta = 135°$) under the same cutting parameters ($V_t = 40$ m/min, $f = 35$ kHz, $A = 4$ μm). The maximum length from the cutting edge surface to the deepest damage position was used to represent the surface damage degree L_d; the evaluation mode adopts the maximum failure degree of CFRP caused by cutting process as shown in Fig. 2. In order to ensure the reliability of L_d measurement, the maximum damage degree on the left and right sides of the cutting edge was measured three times, and the average value was taken as the final result.

The variation patterns of CFRP damage degree L_d and fiber orientation angle for different machining methods and the same cutting parameters ($V_t = 40$ m/min, $f = 35$ kHz, $A = 4$ μm) are given in Fig. 2; it can be seen from the figure that the introduction of ultrasonic reduces the damage degree of CFRP to varying degrees, and the damage degree of CFRP under torsional vibration mode is the smallest. With the change of fiber angle, the change trend of damage degree characteristic L_d is similar no matter which processing method is used. When $0° < \theta < 90°$, the damage degree of the three different machining methods increases with the increase of the fiber cutting angle, and the damage degree L_d reaches the maximum value near $\theta = 90°$. When $\theta > 90°$, the degree of damage shows a decreasing trend. The reason is that when CFRP is processed in different ways, the instantaneous cutting force of cutting fiber is different, resulting in different damage changes.

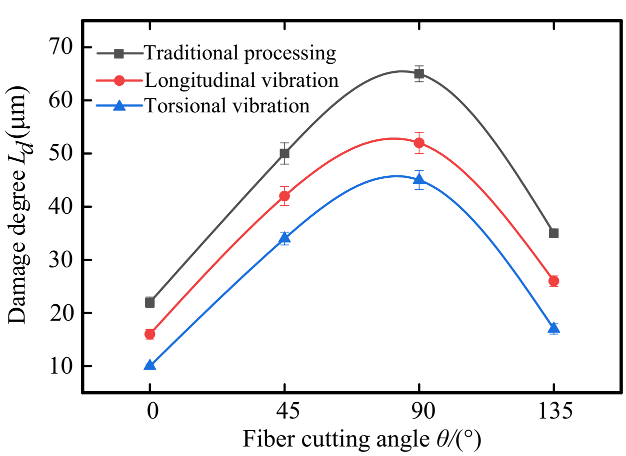

Fig. 2 CFRP damage degree varies with "θ"

Figure 3 shows the damage analysis of vertical cutting CFRP under different machining methods and the same machining parameters ($V_t = 40$ m/min, $f = 35$ kHz, $A = 4$ μm). It can be seen from Fig. 3a that traditional cutting has the most damage, a large range of matrix debonding occurred on both sides of the material contacted by the tool tip, the debonding point of the fiber matrix is far away from the cutting edge of the tool, the failure area of the resin matrix around the cutting edge is large, and after the partially failed substrate falls off, the substrate adheres to the cutting edge due to cutting heat and moves simultaneously with the feed of the cutting edge. In Fig. 3b, the debonding point is closest to the tool fiber contact point, and matrix failure rarely occurs, but the CFRP around the tool has holes, which does not appear in other processing methods. In Fig. 3c, the tool additional longitudinal vibration debonding point is closer to the tool fiber contact point than the traditional processing, there are few matrix failures in the local state after amplification, and there is almost no matrix bonding tool.

Figure 4 shows the damage analysis of cutting CFRP at a fiber cutting angle of $\theta = 45°$ under different processing methods and the same processing parameters ($V_t = 40$ m/min, $f = 35$ kHz, $A = 4$ μm). It can be seen from the figure that different degrees of resin matrix cracking occurred between processed fiber and processed CFRP under the three processing methods. Due to the plastic deformation of CFRP matrix, the processed material has rebound phenomenon, so the interlaminar cracking phenomenon at other positions of the processed material is significantly weakened, especially when the vibration direction in Fig. 4c is perpendicular to the cutting direction.

Figure 5 shows the damage analysis of cutting CFRP at a fiber cutting angle of $\theta = 135°$ under different processing methods and the same processing parameters ($V_t = 40$ m/min, $f = 35$ kHz, $A = 4$ μm). It can be seen from Fig. 5a that cracking occurs between fibers just below the tool tip in traditional cutting, while no interlayer cracking is found in the other two machining methods. During the torsional vibration machining in Fig. 5b, a cavity appears under the tool tip due to the impact force of the tool. The fibers near the cutting angle of this fiber are subject to bending deformation under the action of cutting force, mainly bending fracture.

3 Test conditions and test plan

The test material is T300 CFRP unidirectional laminate with a thickness of 5 mm and 40 plies. In order to better simulate the orthogonal cutting test of 0° ~ 180° ~ 360° all fiber

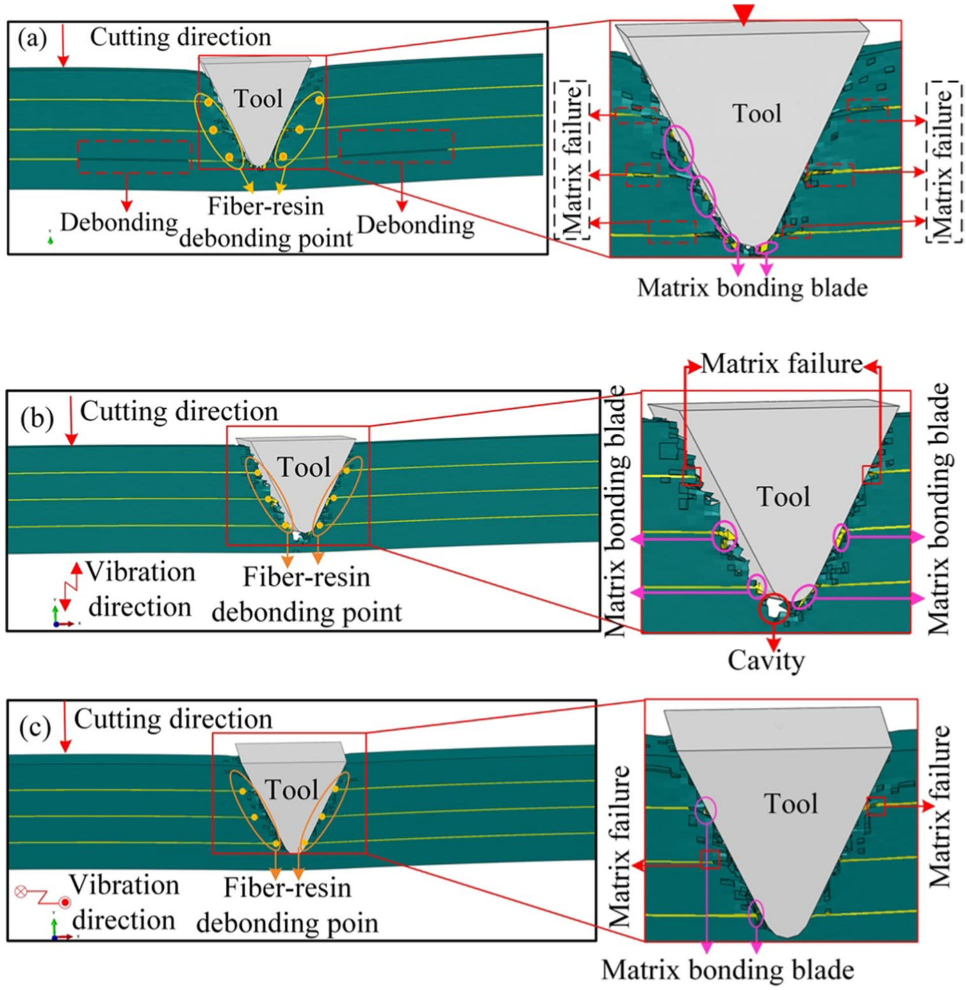

Fig. 3 CFRP defect analysis ($\theta=90°$). **a** Ordinary cutting. **b** Torsional ultrasonic-assisted cutting. **c** Longitudinal ultrasonic-assisted cutting

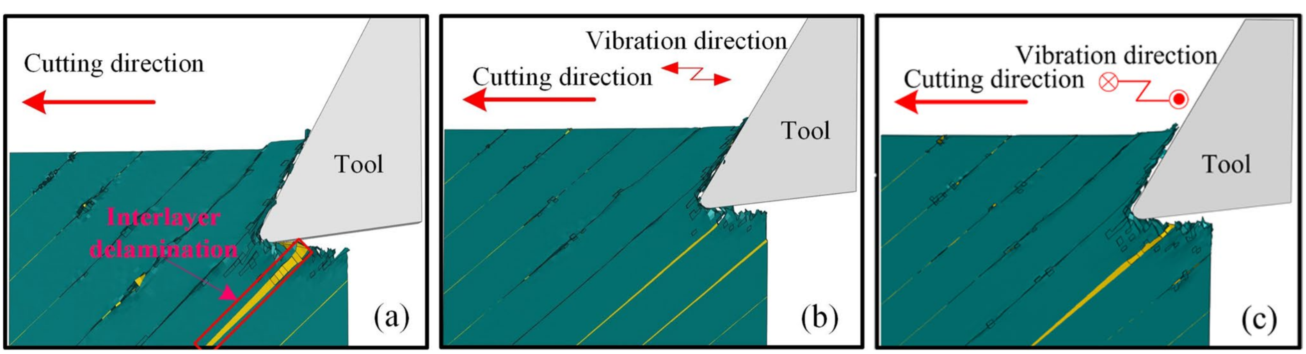

Fig. 4 CFRP defect analysis ($\theta=45°$). **a** Ordinary cutting. **b** Torsional ultrasonic-assisted cutting. **c** Longitudinal ultrasonic-assisted cutting

cutting angle, the material was processed into a disc workpiece with a diameter of 100 mm. In order to ensure the uniformity of the fiber bonding strength, 1.5 mm was removed from both sides of the disc, and 2 mm was removed from the radial circumference of the circle, so that a convex table with a thickness and height of 2 mm was formed around the circumference of the CFRP disc; a 2-mm notch was machined on the circumference of the disc to mark the position of each cutting angle. Table 2 shows the composition of the workpiece material CFRP (T300-12 K/AG80); Table 3 shows the physical/mechanical properties of workpiece materials. The tool used in the test is diamond PCD lathe blade (Model: DCMT07020), the geometric parameters of the tool are consistent with those in the simulation, and the radius of the

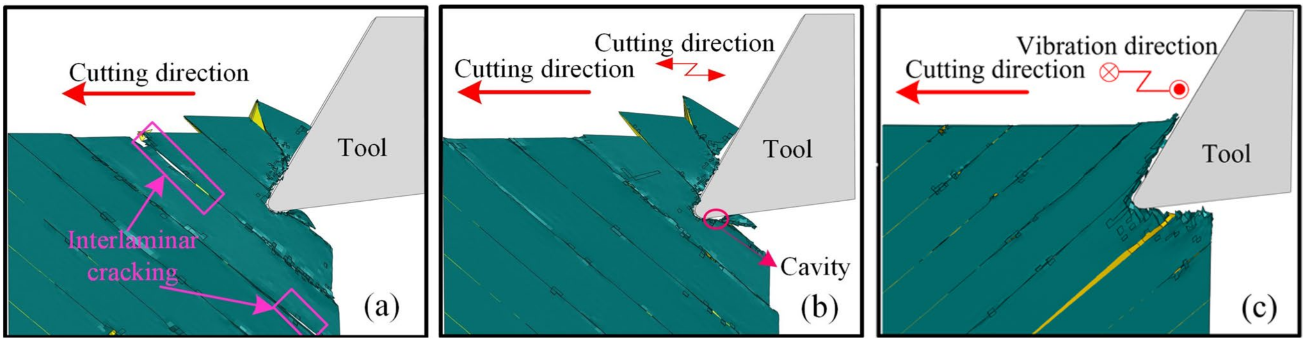

Fig. 5 CFRP defect analysis ($\theta = 135°$). **a** Ordinary cutting. **b** Torsional ultrasonic-assisted cutting. **c** Longitudinal ultrasonic-assisted cutting

Table 2 Composition of CFRP laminates

Reinforced material	Matrix material	Density/g/cm^3	Fiber volume fraction/	Average fiber diameter/μm
T300	AG80	1.76	60	7

Table 3 CFRP mechanical/physical properties

Tensile strength/MPa	Tensile modulus/GPa	Elongation/%
3530	230	1.5

blade blunt circle is about 5 ~ 10 μm, which is basically the same as the diameter of a single filament.

The test was carried out on the sphere360 ultra precision diamond lathe; the AE sensor was used to collect and monitor the processing status and the fracture form of the fiber online. The ultrasonic vibration system used in the test includes the following: the 35 kHz ultrasonic generator developed by the research group, piezoelectric ceramic transducer, and one-dimensional vibrating conical horn designed according to the test requirements. The test site of ultrasonic-assisted orthogonal cutting of CFRP disc is shown in Fig. 6. In order to simulate the vibration of the main cutting edge of the tool in contact with the fiber in the process of longitudinal-torsional ultrasonic-assisted cutting, the CFRP of longitudinal-torsional ultrasonic-assisted cutting was decomposed into longitudinal ultrasonic vibration of the tool and torsional ultrasonic vibration of the tool.

According to the actual processing conditions, the ultrasonic-assisted orthogonal cutting test of the CFRP unidirectional lamination plate disc takes three different processing modes as the processing mode factors investigated in this test: ordinary mode, tool-added torsional vibration, and tool-added longitudinal vibration. Taking fiber cutting angle, cutting speed, and ultrasonic amplitude as the processing parameter factors investigated in this test. In order to reduce the impact of tool wear on the machining results, a new blade shall be replaced every time a parameter is changed for machining, so as to ensure the reliability and comparability of each group of test data. The test parameters are shown in Table 4. Analyze the surface quality of processed CFRP after the test; the surface roughness index R_a of the machined surface of CFRP disc was measured by Beijing time 3221 probe surface roughness instrument. The sampling length is 0.8 mm, the number of samples is 4, and the measurement distance is 3.2 mm. The machined surface morphology of the circumference of CFRP disc was observed by SEM scanning electron microscope, the disc workpiece was fixed by a special fixture, and the workpiece can be rotated during observation to obtain the surface topography of any fiber angle.

The surface morphology of 90° fiber cutting angle was observed by SEM, as shown in Fig. 7, Fig. 7a shows the typical morphology of pits formed by bending and fracture near the fiber cutting angle of 90° during traditional processing, and Fig. 7b shows the typical morphology of smooth plane formed by shear fracture near 90° of fiber cutting angle during torsional ultrasonic-assisted machining. It can be seen from Fig. 7 that there are many damages during traditional cutting, and the fiber-resin debonding has a serious expansion phenomenon, and fibers are mainly bent and broken. In the process of ultrasound-assisted cutting, the larger instantaneous concentrated energy generated by ultrasonic impact force promotes the rapid fracture of fiber, inhibits the generation and expansion of debonding phenomenon, and the matrix failure phenomenon is less, which indicates that ultrasonic machining can effectively inhibit the surface damage of CFRP. The experimental results are in good agreement with the simulation results.

4 Analysis and discussion of test results

In order to investigate the weakening effect of processing parameters and processing methods on the fiber direction of the processed surface quality, the difference I between the

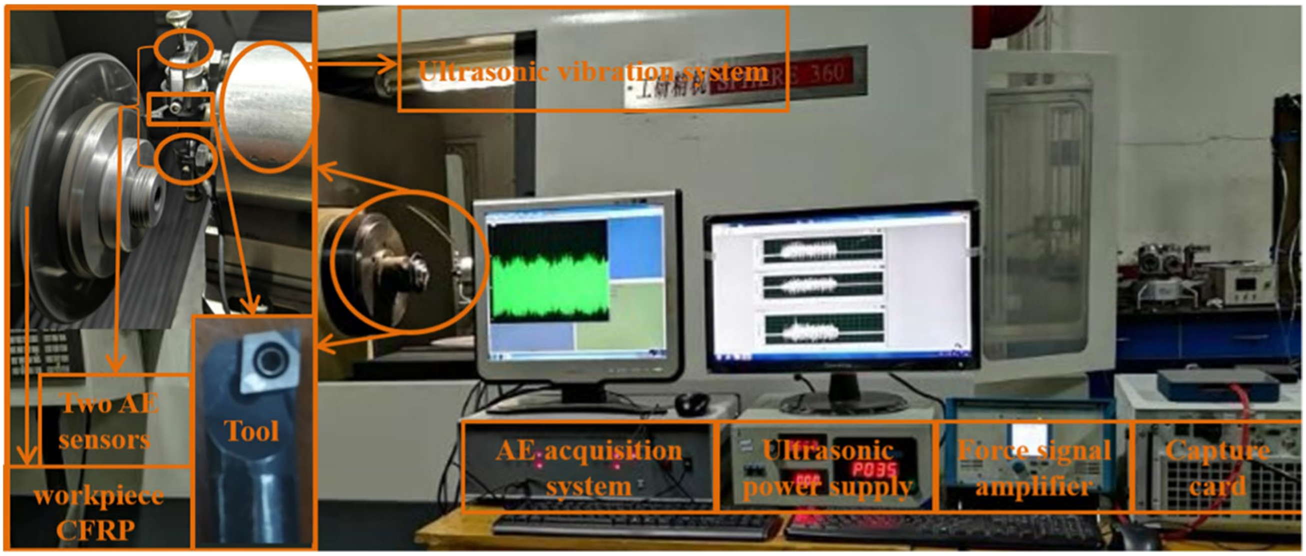

Fig. 6 Ultrasonic-assisted orthogonal cutting CFRP disc test device and test tool

Table 4 Test parameter

Machining parameter	Level
Spindle speed (r/min)	110,166,221,276
Ultrasonic amplitude (μm)	0,2,4,6

maximum and minimum roughness in a cutting fiber angle cycle is taken as the index of weakening the influence of fiber directivity, the incremental parameter $I = Ra_{max}$-Ra_{min}, under normal circumstances, when the value of I is small, the directionality of the fiber is not obvious; on the contrary, the directionality is more significant.

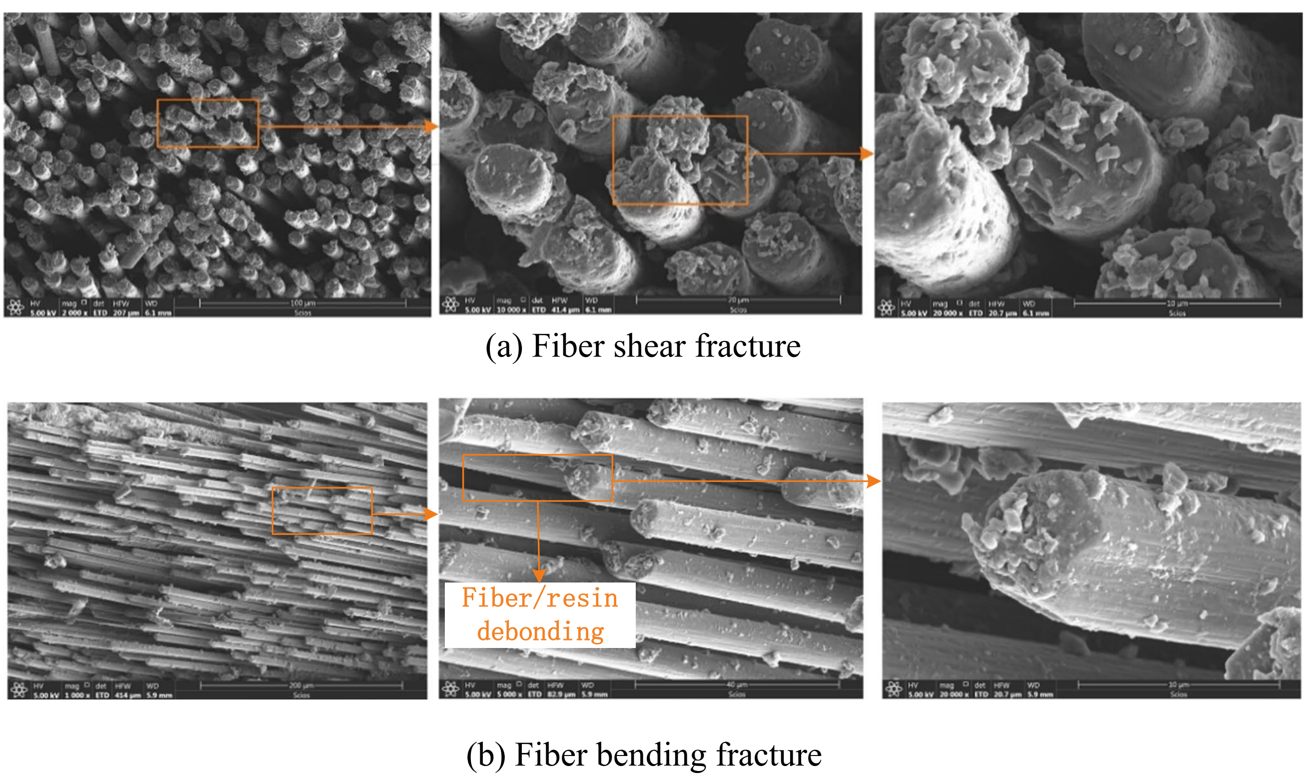

Fig. 7 CFRP surface by SEM

4.1 Effect of cutting speed on surface quality

Figure 8 shows the change curve of surface roughness index R_a with fiber cutting angle under different cutting speeds in the traditional processing mode. It can be seen that the surface roughness value presents two larger values in a disc cutting cycle, in the first and third quadrants; the surface quality is relatively good in the second and fourth quadrants. When the speed is $n = 110$ r/min, the surface quality deteriorates rapidly, and fiber directivity is abnormal and significant. At this time, $I = 9.68$, while the roughness increment I decreases with the increase of speed. It can be seen that the roughness increment parameter I decreases with the increase of the speed; that is, high-speed machining can effectively weaken the directionality of the fiber.

Figure 9 shows the additional torsional vibration of the tool ($A = 4$ μm. $f = 35$ kHz); the change curve of cutting speed to surface roughness with fiber direction angle, compared with traditional processing, and the addition of torsional vibration effectively reduce the surface roughness; at the same time, the separation between the workpiece and the tool occurs when $n < 2\pi fA$. The reason is that the torsional vibration reduces the deflection curvature when the fiber breaks, the instantaneous high-energy impact force makes the fiber shear fracture before bending deformation occurs, the fracture energy of fibers mainly comes from the action of ultrasonic, and the effect of speed is no longer significant, so with the change of speed, the surface quality does not change much.

By analyzing the roughness increment parameter I in Fig. 9, it is found that the ultrasonic processing is reduced compared with the traditional processing at the same processing speed, especially in the low-speed machining area; the increment parameter decreases significantly, indicating that ultrasonic plays a better role in the low-speed area. When $n > 2\pi fA$, that is, $n = 276$ r/min, the roughness value and increment parameter I increase rapidly, and the influence of fiber directivity on surface quality increases. When $n < 2\pi fA$ is processed at low-speed, the contribution of ultrasonic action to fiber fracture is prominent, the surface quality is relatively good, and the influence of directivity is also well suppressed.

Figure 10 shows the additional longitudinal vibration of the tool ($A = 4$ μm. $f = 35$ kHz) at different speeds; the change of cutting speed on surface roughness with fiber direction angle and the improvement of the sharpness of

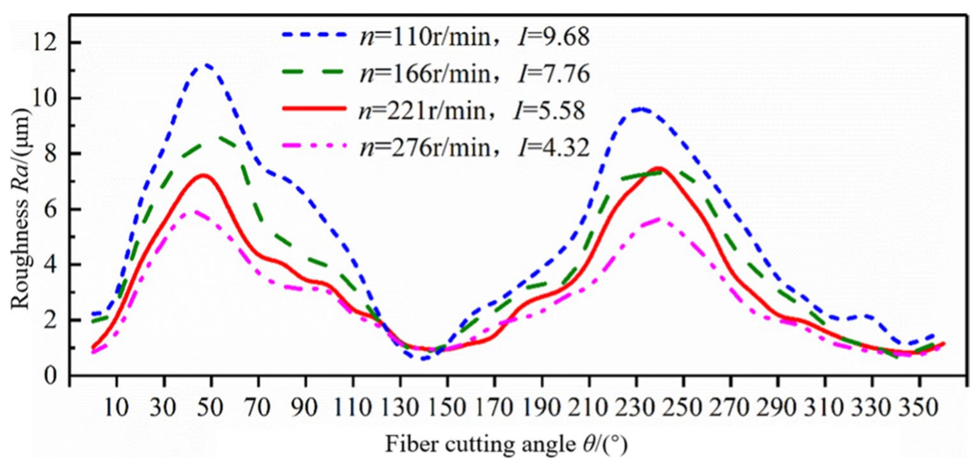

Fig. 8 Relationship between roughness and speed with "θ" under traditional machining

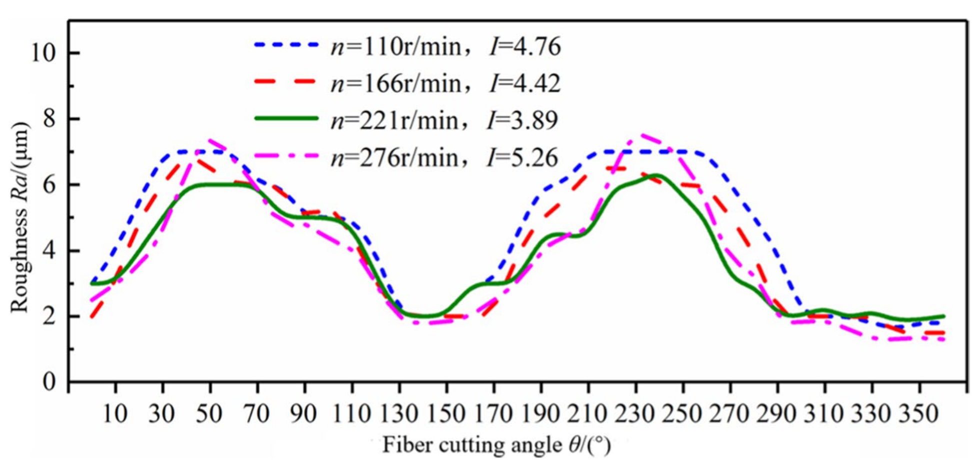

Fig. 9 Relationship between roughness and speed with "θ" under torsional vibration

the cutting tool in this way leads to the reduction of the contact area between the cutting edge of the tool and the fiber. When the cutting force acts, the internal stress of the fiber in the contact area increases and quickly reaches the fracture limit, and the extrusion fracture of fibers reduces the occurrence of damage, thereby effectively improving the surface quality.

By comparing the roughness increment parameter I at the same speed in Figs. 9 and 10, it is found that the influence range of longitudinal vibration processing on roughness is smaller than that of torsional vibration; with the increase of velocity, the change of roughness increment parameter I during longitudinal ultrasonic vibration shows a slightly decreasing trend.

4.2 (2) Effect of ultrasonic amplitude on surface quality

Figure 11 shows the change of ultrasonic amplitude on surface roughness with fiber direction angle when the tool is subjected to additional torsional vibration ($n = 110$ r/min, $f = 35$ kHz). It can be seen from the figure that the surface roughness decreases significantly with the increase of amplitude; however, when the amplitude is small, the effect of ultrasonic does not show any advantage; the reason is that at this time, the critical speed of ultrasonic is low, the rotational linear velocity of the workpiece is greater than the critical speed of ultrasonic, and the effect of ultrasonic disappears. As with the traditional processing method, the fiber fracture is mainly due to the effect of speed. The roughness increment parameter I is analyzed; with the increase of amplitude, the value of I decreases rapidly; it shows that the greater the amplitude is in a certain range, the more obvious the inhibition of the influence on fiber directivity.

5 Conclusions

Through the establishment of finite element simulation model of ultrasonic-assisted cutting CFRP and the experiment of ultrasonic-assisted cutting CFRP disc, the influence mechanism of machining methods and processing parameters on CFRP surface quality is explored. The main conclusions are as follows:

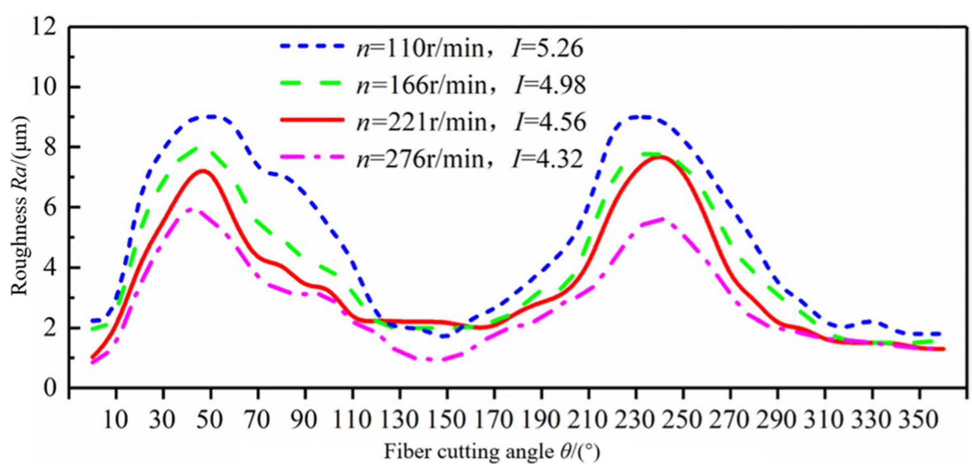

Fig. 10 Relationship between roughness and speed with "θ" under longitudinal vibration

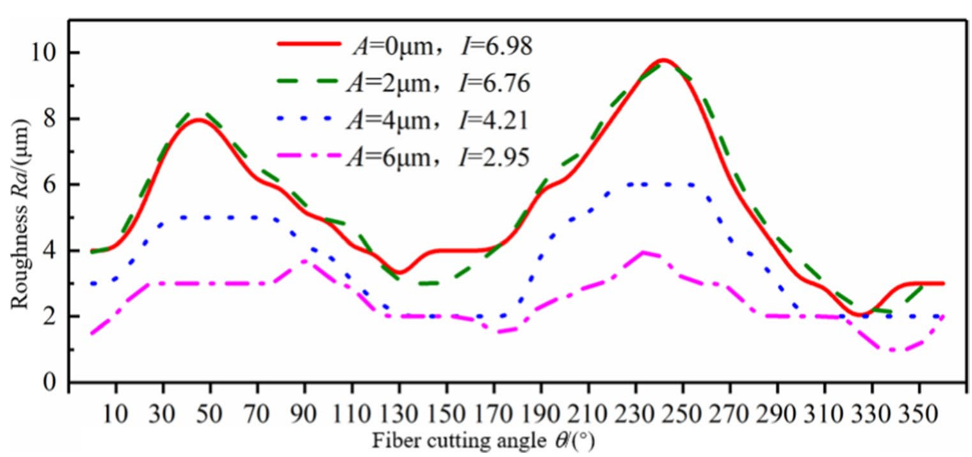

Fig. 11 Relationship between roughness and amplitude with "θ" under torsional vibration

- The simulation results show that the damage degree of CFRP is reduced by the introduction of ultrasonic; the surface quality of torsional ultrasonic-assisted machining is the best, followed by longitudinal ultrasonic-assisted machining. Fiber cutting angle has significant influence on material machining damage.
- The experimental results show that the introduction of ultrasonic changes the fracture mode of fiber and can effectively reduce the surface roughness value, especially when the tool is subject to additional torsional vibration, the fiber removal method is given priority to with shear fracture, and the surface roughness value of the area with severe pits decreases by about 4 ~ 6 μm.
- The fiber cutting angle is the main factor affecting the roughness of CFRP cutting surface. The ultrasonic effect is better in the low-speed area, and the influence of fiber directivity will be weakened in the high-speed machining.
- Ultrasonic-assisted machining has changed the material removal mechanism in CFRP cutting process. Large amplitude and small cutting speed can obtain better ultrasonic machining effect, and large amplitude and high cutting speed can effectively inhibit the influence of fiber directivity.

Author contribution Xiaobo Wang: initial draft, funding acquisition; Chaosheng Song: theoretical analysis, methodology; Jinglin Tong: writing editing, paper format arrangement; Lulu Li: picture arrangement; Mingqiang Wu: paper format arrangement; Bo Zhao: writing—eview and editing.

Funding This research is supported by the national Natural Science Foundation of China project "Research on subsurface damage mechanism of ceramic matrix composites machined by high speed multi-dimensional ultrasonic" (Project code: 52005164).

Data availability Not applicable.

Code availability Not applicable.

Declarations

Ethics approval Not applicable.

Consent to participate Not applicable.

Consent for publication Not applicable.

Conflict of interest The authors declare no competing interests.

References

1. Wang HL (2021) Research on the synchronous development of fiber reinforced composites with new energy vehicles. Synth Mater Ageing Appl 50:134–136
2. Peng PC, Xiang DH, Li YQ, Yuan ZJ, Lei XF, Li B, Liu GF, Zhao B, Gao GF (2022) Experimental study on laser assisted ultrasonic elliptical vibration turning (LA-UEVT) of 70% SiCp/Al composites. Ceram Int 48:33538–33552. https://doi.org/10.1016/j.ceramint.2022.07.298
3. Zimmermann N, Wang PH (2020) A review of failure modes and fracture analysis of aircraft composite materials. Eng Fail Anal 115:104692. https://doi.org/10.1016/j.engfailanal.2020.104692
4. Soutis C (2005) Fibre reinforced composites in aircraft construction. Prog Aerosp Sci 41:143–151. https://doi.org/10.1016/j.paerosci.2005.02.004
5. Gao T, Li CH, Jia DZ, Zhang YB, Yang M, Wang XM, Cao HJ, Li RZ, Ali HM, Xu XF (2020) Surface morphology assessment of CFRP transverse grinding using CNT nanofluid minimum quantity lubrication. J Clean Prod 277:123328. https://doi.org/10.1016/j.jclepro.2020.123328
6. Gao T, Li CH, Wang YQ, Liu XS, An QL, Li HN, Zhang YB, Cao HJ, Liu B, Wang DZ, Said Z, Debnath H, Jamil M, Ali HM, Sharma S (2022) Carbon fiber reinforced polymer in drilling: From damage mechanisms to suppression. Compos Struct 286:115232. https://doi.org/10.1016/j.compstruct.2022.115232
7. Abootorabi Zarchi MM, Razfar MR, Abdullah A (2012) Investigation of the effect of cutting speed and vibration amplitude on cutting forces in ultrasonic-assisted milling. Proc Inst Mechl Eng, Part B: J Eng Manuf 226(7):1185–1191. https://doi.org/10.1177/0954405412439666
8. Amini S, Soleimani M, Paktinat H, Lotfi M (2017) Effect of longitudinal− torsional vibration in ultrasonic-assisted drilling. Mater Manuf Proc 32(6):616–622. https://doi.org/10.1080/10426914.2016.1198027
9. Yang YY, Yang M, Li CH, Li RZ, Said Z, Ali HM, Sharma S (2022) Machinability of ultrasonic vibration assisted micro-grinding in biological bone using nanolubricant. Front Mech Eng. https://doi.org/10.1007/s11465-022-0717-z
10. Kang RK, Ma FJ, Dong ZG, Guo DM (2012) Ultrasonic assisted machining of difficult-to-cut material. Aeronaut Manuf Tech 16:44–49
11. Gao W, Liu B, Yao JZ (2018) Application and Research on ultrasonic-assisted processing of carbon fiber composites. Mechanical Enginee 12:130-131 134
12. Gao T, Zhang YB, Li CH, Wang YQ, Chen Y, An QL, Zhang S, Li HN, Cao HJ, Ali HM, Zhou ZM, Sharma S (2022) Fiber-reinforced composites in milling and grinding: machining bottlenecks and advanced strategies. Front Mech Eng 17(2):1–35. https://doi.org/10.1007/s11465-022-0680-8
13. Patil S, Joshi S, Tewari A, Joshi SS (2013) Modelling and simulation of effect of ultrasonic vibrations on machining of Ti6Al4V. Ultrasonics 54:694–705. https://doi.org/10.1016/j.ultras.2013.09.010
14. Muhammad R, Hussain MS, Maurotto A, Siemers C, Roy A, Silberschmidt VV (2014) Analysis of a free machining α+β titanium alloy using conventional and ultrasonically assisted turning. J Mater Process Technol 214:906–915. https://doi.org/10.1016/j.jmatprotec.2013.12.002
15. Liu Y, Liu ZB, Wang XB, Huang T (2021) Experimental study on cutting force and surface quality in ultrasonic vibration-assisted milling of c/sic composites. Int J Adv Manuf Tech 112:2003–2014. https://doi.org/10.1007/s00170-020-06355-x
16. Zhang X, Chen Y, Hu J (2018) Recent advances in the development of aerospace materials. Prog Aerosp Sci 97:22–34. https://doi.org/10.1016/j.paerosci.2018.01.001
17. Sun MH, Guo YQ, Tang PP, Yan Y (2015) Study on shear fracture behavior of carbon fiber-reinforced plastic composites. Mater Rep 29:64-68 81
18. Lou SW, Liang GX, Ma ZF, Lv M. (2021) Effect of grinding fiber angle on grinding performance of carbon fiber composites. Machinery Design & Manufacture, 91–93+97.

19. Chen J, Ming WW, An QL, Chen M (2020) Mechanism and feasibility of ultrasonic-assisted milling to improve the machined surface quality of 2D C_f/SiC composites. Ceram Int 46(10):15122–15136. https://doi.org/10.1016/j.ceramint.2020.03.047
20. Ik B (2008) Experimental investigations of surface roughness in orthogonal turning of unidirectional glass-fiber reinforced plastic composites. Int J Adv Manuf Technol 37:2–48. https://doi.org/10.1007/s00170-007-0946-7
21. Ik B, Ekici E (2010) Experimental investigations of damage analysis in drilling of woven glass fiber-reinforced plastic composites. Int J Adv Manuf Tech 49:861–869. https://doi.org/10.1007/s00170-009-2440-x
22. Shen GL, Hu GK. (2013) Chanics of composite materials. Beijing: qinghua University Press, 68–69.
23. Guden M, Yildirim U, Hall IW (2004) Effect of strain rate on the compression behavior of a woven glass fiber/sc-15 composite. Polym Testing 23:719–725. https://doi.org/10.1016/j.polymertesting.2004.01.004
24. Hosur MV, Alexander J, Vaidya UK, Jeelani S, Mayer A (2004) Studies on the off-axis high strain rate compression loading of satin weave carbon/epoxy composites. Compos Struct 63:75–85. https://doi.org/10.1016/S0263-8223(03)00134-X
25. Zhao B, Zhao L, Xu HL (2012) The research about damage of composite laminate in bolted joints based on the Hashin failure criteria. Sci Tech Eng 12:1740–1744
26. Kermanidis T, Labeas G, Tserpes KI, Pantelakis S. (2000) Finite element modelling of damage accumulation in bolted composite joints under incremental tensile loading.
27. Tserpes KI, Labeas G, Papanikos P, Kermanidis T (2002) Strength prediction of bolted joints in graphite/epoxy composite laminates. Compos B Eng 33:521–529. https://doi.org/10.1016/S1359-8368(02)00033-1
28. Matzenmiller A, Lubliner J, Taylor RL (1995) A constitutive model for anisotropic damage in fiber-composites. Mech Mater 20:125–152. https://doi.org/10.1016/0167-6636(94)00053-0
29. Liu HX, Jiao GQ, Xiong W, Guan G (2008) Analysis of delamination with interface element in composite materials. J Mech Strength 30:301–304
30. Harper PW, Hallett SR (2008) Cohesive zone length in numerical simulations of composite delamination. Eng Fract Mech 75:4774–4792. https://doi.org/10.1016/j.engfracmech.2008.06.004